PSIG 2430

Real-Time Transient Modeling of CO_2 Pipelines and Phase Behavior During the Leak

Hamed Ghasvari-Jahromi [1] *, *Fatemeh Ekram* [1], *Satya Mokamati* [1]

[1] *Vanmok Leak Detection Technologies Inc., Canada*

* *E-mail: hamed@vanmok.com*

This paper was prepared for presentation at the PSIG Annual Meeting held in Charleston, South Carolina, 7 May – 10 May 2024.

ABSTRACT

A clear understanding of flow characteristics of CO_2 pipelines under various operating conditions, including leaks, provides valuable insights for effective monitoring and design of reliable leak detection systems. In this paper, we address the challenges of real-time transient modeling of CO_2 pipelines. The proposed modeling framework integrates the compressible flow dynamics and phase transitions to study the complex phenomenon of CO_2 release. The approach and findings of this paper contribute to enhancing leak detection in pipelines and help with mitigating emissions of greenhouse gases accordingly.

1 INTRODUCTION AND BACKGROUND

CO_2 pipelines are a key component of carbon capture, utilization, and storage (CCUS) initiatives. These pipelines are being expanded to facilitate the transfer of captured CO_2 from industrial sources to designated storage sites.

Utilizing dynamic modeling for CO_2 transportation pipelines offers a robust tool for ensuring the safety and efficiency of pipeline operations while minimizing the social and environmental impacts in the event of a leak. A comprehension of the flow dynamics within CO_2 pipelines across diverse operational scenarios, encompassing instances such as leaks, offers invaluable insights crucial for the development and implementation of robust leak detection systems, as well as for optimizing pipeline design for enhanced reliability.

While transporting CO_2 in the supercritical or dense phase is the most economically efficient practice, our paper takes a comprehensive approach by considering CO_2 flow in gas, liquid, and supercritical states. This approach allows us to provide valuable observations and analyses to examine pipeline behavior under different operating conditions and during a leak.

Within this paper, we discuss the mathematical modeling of CO_2 pipeline and validate the presented model using case studies from literature. A novel approach is used for on-line calculation of the fluid properties, ensuring the numerical stability of the system around the critical point and throughout the supercritical region.

Additionally, we conduct simulations to replicate the complex phenomenon of CO_2 pipeline leakage. The simulated leak predictions are cross-referenced with the experimental results available in the literature to ensure alignment between our predictions and performed numerical analysis with real-world data and observations.

We demonstrate the temperature evolution and the formation and propagation of pressure waves at the moment of the rupture and at different time intervals following the release. Furthermore, we analyze the trajectory of the thermodynamic properties and thoroughly examine the underlying phase transitions during the CO_2 leak. Lastly, the effects of the choked flow at the leak location and the corresponding maximum flow rate are presented.

The approach and findings outlined in this paper not only contribute to enhancing the detection of leaks in CO_2 pipelines transporting fluids like natural gas, LNG and LPG, thus mitigating emissions of methane and other greenhouse gases.

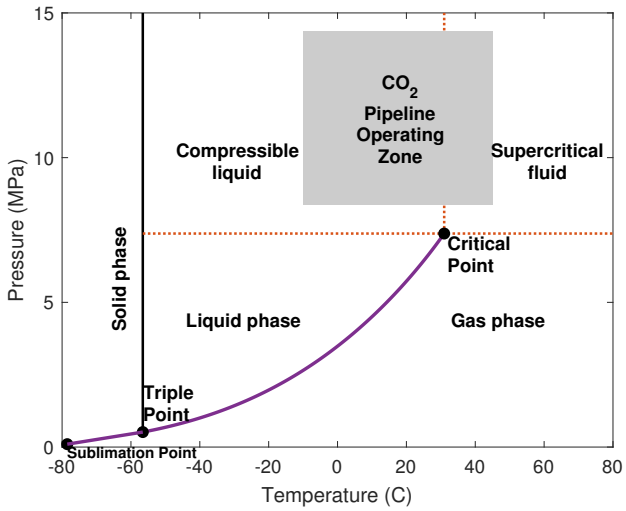

Figure 1 CO_2 **Phase Diagram.**

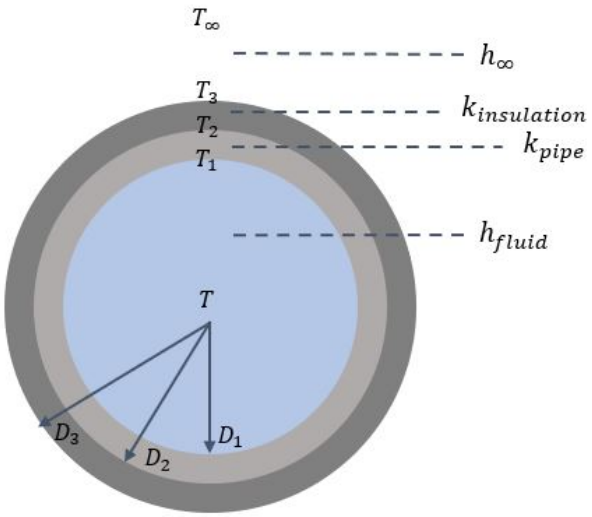

Figure 2 The pipe cross-section showing the thermal layers.

2 MODELING OF CO_2 PIPELINES

In order to achieve an accurate prediction of CO_2 behavior in a pipeline, advanced mathematical models are necessary. These models encompass various aspects of fluid flow, such as turbulence, compressibility, phase transitions, and heat transfer mechanisms, including conduction, convection, and radiation. Integration of these models with empirical data and computational fluid dynamics (CFD) simulations facilitates the development of a comprehensive understanding of the complex hydrodynamic and heat transfer processes prevalent within pipeline systems.

2.1 Governing Equations of the Mathematical Model

The equations of mass, momentum and energy for one-dimensional compressible flow in a pipeline are presented in equations 2.1, 2.2, and 2.3 [1].

$$\frac{\partial \rho}{\partial t} + \frac{\partial(\rho v)}{\partial x} = 0 \tag{2.1}$$

$$\frac{\partial(\rho v)}{\partial t} + \frac{\partial(P + \rho v^2)}{\partial x} = -\frac{f\rho v|v|}{2D} - \rho g sin\alpha \tag{2.2}$$

$$\frac{\partial}{\partial t}\left[\left(u + \frac{v^2}{2}\right)\rho\right] + \frac{\partial}{\partial x}\left[\left(h + \frac{v^2}{2}\right)\rho v\right] = \rho q - \rho v g sin\alpha \tag{2.3}$$

Equation 2.2 can be rewritten using equation 2.1 into 2.4.

$$\frac{dv}{dt} + \frac{1}{\rho}\frac{\partial(P)}{\partial x} + \frac{f v|v|}{2D} + g sin\alpha = 0 \tag{2.4}$$

Equation 2.5 was obtained after substituting equations 2.1 and 2.4 into the equation 2.3 and rearranging.

$$\rho\frac{dh}{dt} - \frac{dP}{dt} + \frac{f\rho v^3}{2D} = \rho q \tag{2.5}$$

Using equations 2.6 and 2.7, we can rewrite the equations 2.1, 2.4 and 2.5 with pressure, temperature and mass flow rate as the dependent variables. Equition 2.8 represents enthalpy.

$$v = \frac{\dot{m}}{\rho A} \tag{2.6}$$

$$d\rho = \left(\frac{\partial \rho}{\partial T}\right)_P dT + \left(\frac{\partial \rho}{\partial P}\right)_T dP \tag{2.7}$$

$$dh = c_p dT + \left[1 + \frac{T}{\rho}\left(\frac{\partial \rho}{\partial T}\right)_P\right]\frac{dP}{\rho} \tag{2.8}$$

The continuity, momentum and energy equations in terms of pressure (P), temperature (T) and mass flow rate ($\dot{m}$) are presented in equations 2.9, 2.10 and 2.11.

$$\left(\frac{\partial \rho}{\partial P}\right)_T \frac{\partial P}{\partial t} + \left(\frac{\partial \rho}{\partial T}\right)_P \frac{\partial T}{\partial t} = -\frac{1}{A}\frac{\partial \dot{m}}{\partial x} \tag{2.9}$$

$$\begin{aligned}\frac{1}{A}\frac{\partial \dot{m}}{\partial t} = &\left[\left(\frac{\dot{m}}{\rho A}\right)^2\left(\frac{\partial \rho}{\partial P}\right)_T - 1\right]\frac{\partial P}{\partial x} - \frac{2\dot{m}}{\rho A^2}\frac{\partial \dot{m}}{\partial x} \\ &+ \left(\frac{\dot{m}}{\rho A}\right)^2\left(\frac{\partial \rho}{\partial T}\right)_P \frac{\partial T}{\partial x} - \frac{2f\dot{m}|\dot{m}|}{D\rho A^2} - \rho g sin\alpha\end{aligned} \tag{2.10}$$

$$\begin{aligned}\frac{T}{\rho}\left(\frac{\partial \rho}{\partial T}\right)_P \frac{\partial P}{\partial t} + \rho c_p \frac{\partial T}{\partial t} = &-\frac{\dot{m}T}{\rho^2 A}\left(\frac{\partial \rho}{\partial T}\right)_P \frac{\partial P}{\partial x} \\ &- \frac{c_p \dot{m}}{A}\frac{\partial T}{\partial x} + \frac{2f\dot{m}^3}{D\rho^2 A^3} - \frac{h_{fluid}}{A}(T - T_1)\end{aligned} \tag{2.11}$$

$\overline{h}_{fluid}$ and $\overline{h}_{\infty}$ are the convection heat transfer coefficients for the gas and the ambient air respectively. k_{pipe} and $k_{insulation}$ are the thermal conductivity of the pipe wall and the insulation layer. Figure 2 shows these layers as heat capacitors.

$$\frac{m_1 c_{p1}}{dx}\frac{\partial T_1}{\partial t} = \pi D_1 \overline{h}_{fluid}(T - T_1) - \frac{2\pi k_{pipe}}{ln\left(\frac{D_2}{D_1}\right)}(T_1 - T_2)$$
$$\frac{m_2 c_{p2}}{dx}\frac{\partial T_2}{\partial t} = \frac{2\pi k_{pipe}}{ln\left(\frac{D_2}{D_1}\right)}(T_1 - T_2) - \frac{2\pi k_{insulation}}{ln\left(\frac{D_3}{D_2}\right)}(T_2 - T_3)$$
$$\frac{m_n c_{pn}}{dx}\frac{\partial T_3}{\partial t} = \frac{2\pi k_{insulation}}{ln\left(\frac{D_3}{D_2}\right)}(T_2 - T_3) - \pi D_3 \overline{h}_{\infty}(T_3 - T_{\infty}) \tag{2.12}$$

The equivalent resistance (R_t) is the summation of the series of thermal resistances and defined in equation 2.13. In more general cases, we may have parallel resistances which has been discussed in [5].

$$R_t = \left(\frac{1}{\pi D_1 h_{fluid}} + \sum_{i=2}^{3}\frac{1}{2\pi k_i} ln\left(\frac{D_i}{D_{i-1}}\right) + \frac{1}{\pi D_3 h_{\infty}}\right) \tag{2.13}$$

The overall heat transfer coefficient can be then calculated from the equivalent resistance $U = 1/(R_t A)$. A and U must be consistent considering $Q = UA\Delta T$. The overall heat transfer coefficient is often nearly constant over a range of operating conditions.

Initiating with the three conservation laws (continuity, momentum, and energy) as well as the equation of state as an auxiliary equation, the numerical solution for hyperbolic partial differential equations (PDEs) can be derived as described in [2, 3, 4]. The heat transfer model was discussed in detail in [5] for dense phase flow in pipeline.

2.2 *Fluid Properties*

Typically CO_2 is transported in its compressible liquid and supercritical state (also known as dense phase). The critical point of CO_2 is 30.98 ºC and 7.38 MPa. Figure 1 shows the CO_2 phase diagram and the pipeline operating zone. Supercritical fluid, characterized by pressures exceeding the critical point, has a higher density than gas and lower viscosity than liquid which allows more throughput with less pressure drop along the pipe.

The fluid properties of the CO_2 pipeline depend on the composition, temperature, and pressure. Figure 3 shows the variation in CO_2 density as a function of the temperature and pressure. Similarly, figure 4 shows the dependency of specific heat ratio to the temperature and pressure.

An auxiliary equation of state will be coupled with the conservational laws, calculating the fluid properties as a function of the pressure and temperature to simulate the transient and compressible flow.

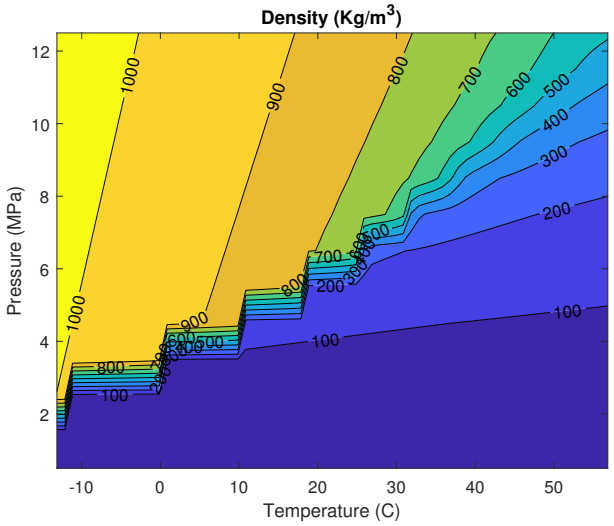

Figure 3 CO_2 density as a function of pressure and temperature. The density values are shown on the figure.

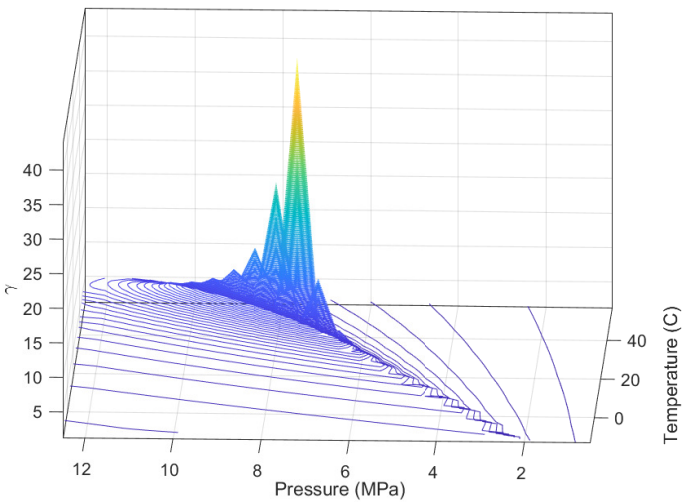

Figure 4 Specific heat ratio as a function of temperature and pressure.

As we discussed in [5], to achieve the best accuracy and minimize the computational effort from an equation of state, the best approach especially for the dense phase fluid in the pipeline is the correctional correlations, which are derived from thermal properties of matter and shaped into thermodynamics functional. This functional becomes an auxiliary equation like a constitutive equation. The data used for obtaining such functional are from Span and Wagner equation of state [6].

The effectiveness of commonly used equation of states for CO_2 and CO_2-mixtures are a matter of discussion [7]. However, accurate calculations of the fluid properties from any of these equation of states are possible when the fluid is far enough from the critical condition. As the fluid passes the critical point, the uncertainties in the calculated properties are increased.

Table 1 Parameters for the reduced density correlation

x	y	R^2	a	b	c	d	k
T_r	ρ_r	0.99	4.43	-3.79	0.99	1.78	-439.5
P_r	ρ_r	1.00	-1.74	2.42	0.59	0.84	1792

Table 2 Parameters for the heat capacity ratio correlation

x	y	R^2	γ_{max}	a	b	c
T_r	γ	0.98	19.97	0.10	1.21	0.62
P_r	γ	0.97	65.85	0.55	1.51	0.66

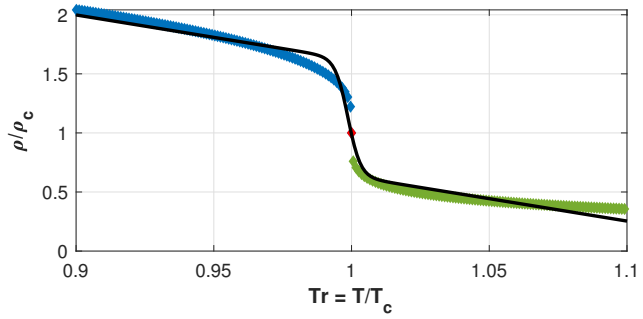

Figure 5 **Reduced density vs reduced temperature at P_{cr} (dots) and the fitted curve (solid line).**

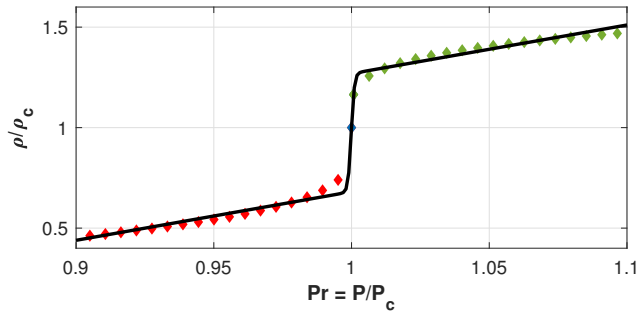

Figure 6 **Reduced density vs reduced pressure at T_{cr} (dots) and the fitted curve (solid line).**

To address the discontinuities of substance properties near the critical point, similar to the proposed method in [5], regularization techniques are employed to determine analytical functions relating CO_2 properties to their reduced temperature and pressure.

Equations 2.14 and 2.15 represent the correlations for reduced density and heat capacity ratio of CO_2, respectively. The parameters for these equations are presented in Table 1 and Table 2.

$$\rho_r = a + bx + \frac{c}{1 + de^{-k(x-1)}} \tag{2.14}$$

$$\gamma = b + |\frac{a}{x-1}|^c \tag{2.15}$$

Figures 5 and 6 show the reduced density vs T_r and P_r, respectively. The heat capacity correlation for T_r and P_r as independent variables are presented in Figures 7 and 8.

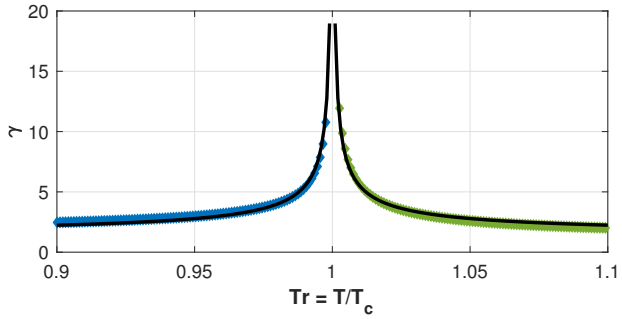

Figure 7 **Heat capacity ratio vs reduced temperature at P_{cr} (dots) and the fitted curve (solid line).**

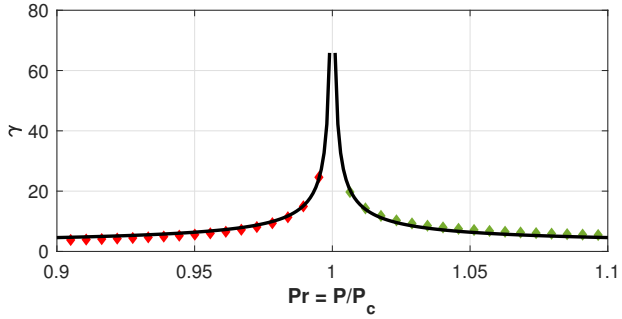

Figure 8 **Heat capacity ratio vs reduced pressure at T_{cr} (dots) and the fitted curve (solid line).**

2.3 Model Verification

In order to verify the model, a case study available in the literature [4] has been used. The set up is 140 km pipeline with no elevation change, transporting high-pressure CO_2 with an outer diameter of 406.4 mm and wall thickness of 12.7 mm.

The boundary conditions employed by Chaczykowski were arbitrary, however carefully selected to represent typical condition for a real CO_2 transportation pipeline used for capture and storage purposes.

The pressure at the outlet is considered to be 10 bar above the critical pressure of $7.38MPa$ for pure CO_2. This ensures the fluid to be in its compressible or supercritical state at all the times during the operation. The inlet temperature is 40 ºC and the ground temperature is 5 ºC. The production rate in the capture plant is variable between 40 to 100 kg/s over 24 hours, as shown in Figure 9, with the linearly increasing rate of $0.25kg/min$ during the transients.

Figure 10 present the calculation of the model for the outlet mass flow rate and inlet pressure, respectively. The results are

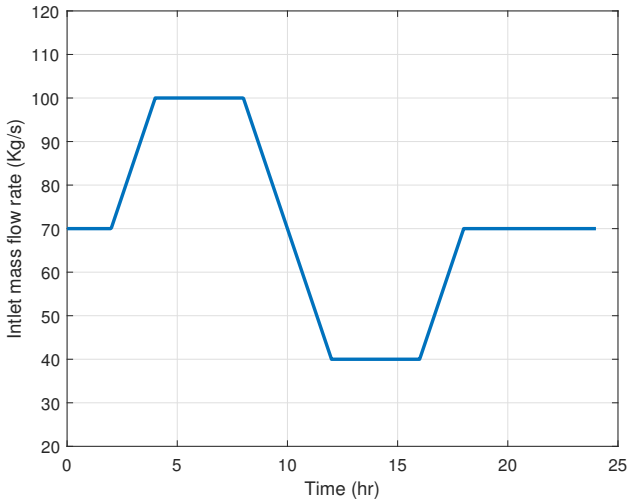

Figure 9 Inlet mass flow rate versus time from [4], applied as the boundary condition for the model.

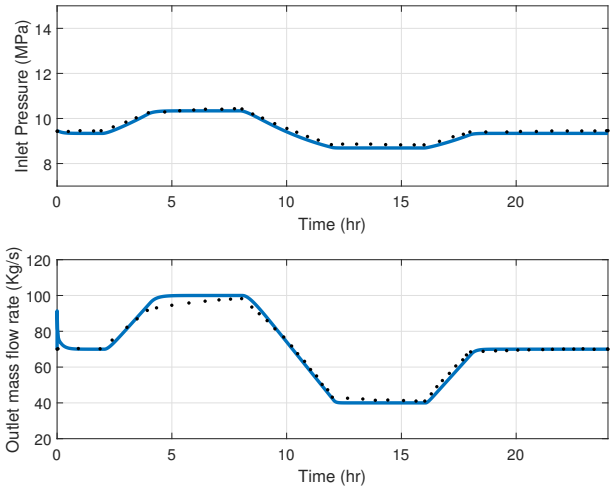

Figure 10 Inlet pressure (top) and outlet mass flow rate (bottom) versus time, calculated by the model (solid blue line) compared to results from [4] (black dots).

in agreement with those obtained in [4], therefore the model can be used to perform the analysis and simulations in the event of the leak.

3 FLOW CHARACTERISTICS DURING THE LEAK

Understanding the phase transitions occurring during the leak is crucial for designing effective leak detection systems. Failure to do so can lead to either false alarms or the leak going undetected [8]. In order to investigate the flow characteristics during a leak from a CO_2 pipeline, the experimental results from the depressurization of a 258 m long pipeline with internal diameter of 233 mm is used as presented in [9]. The pipe was equipped with 50 KW heating tape and 50 mm thermal insulation layer.

Table 3 Description of the experimental conditions

	Gaseous	Dense	Supercritical
Initial pressure (MPa)	3.7	9.0	8.4
Initial temperature (C)	37.5	19.9	35.7
Inventory (tons)	0.85	9.2	6.1
Ambient pressure (MPa)	100.2	100.96	101.34
Ambient temperature (C)	13.5	16.2	16.0
Depressurization time (s)	1620	9200	3300

Table 4 Measurement locations along the pipe

Distance from the orifice (m)	7.4	54.2	237.4	248.6
Color on the P-T diagram	Red	Blue	Green	Purple

The leakage happened through a 15 mm orifice at the end of the pipe, vertically discharged CO_2 to the ambient. The experiments carried out for CO_2 at different phases including gaseous, dense (compressible fluid) and supercritical phases.

The fluid pressure were measured at $10.4m$, $54.2m$, $237.4m$, and $248.6m$, from the leak location along the pipe. The fluid thermocouples were installed at the top and bottom of the pipe at each location to study the changes in the temperature not only along the pipe length but also at the top and bottom of the pipe cross section. More details about the experiment set-up and conduction can be found in [9].

The experimental and environmental conditions during the tests for different initial phases of CO_2 are presented in table 3.

Figures 11, 12 and 13 shows the pressure and temperature evolutions at 4 different locations along the pipe following the leak inception. At each location we have two P-T datasets, one at the top (solid line) and the other at the bottom (dashed line) of the pipe cross-section. Table 4 shows the measurement locations along the pipe and their corresponding colors on the P-T diagrams.

Figure 14 shows Joule-Thomson coefficient which becomes negative for saturated liquid at temperatures below $-30C$. This explains the sudden increase in the temperature when it drops to $-30C$, seen in figure 12 and 13.

The leakage from the pipe full of gaseous CO_2, results in the propagation of the pressure waves to the closed end of the pipe and back to the orifice, repeatedly, while the overall pressure drops as well as the temperature. No phase transition was expected for this test.

At the onset of the leak, during the test with dense phase the pressure and temperature drop to the saturation point of 5.46 MPa and 18 C. The pressure and temperature continue to drop while following the saturation curve for some time before deviating from it and go through phase transition from the liquid-vapor phase to the gaseous phase. As the temperature and pressure decreased to below the triple point,

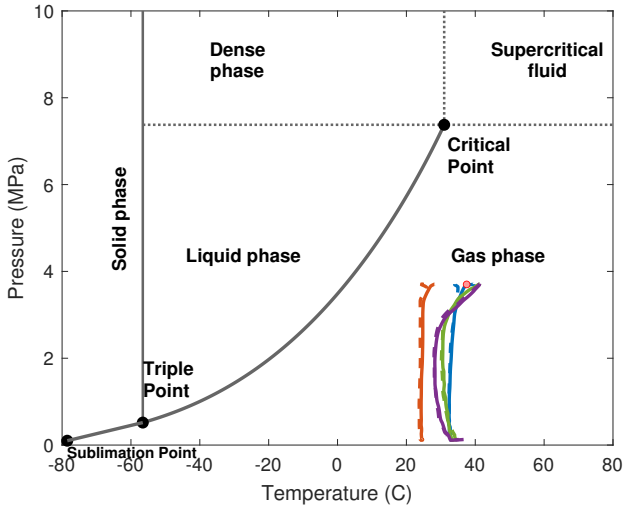

Figure 11 CO_2 **phase diagram showing pressure and temperature during gaseous phase experiment.**

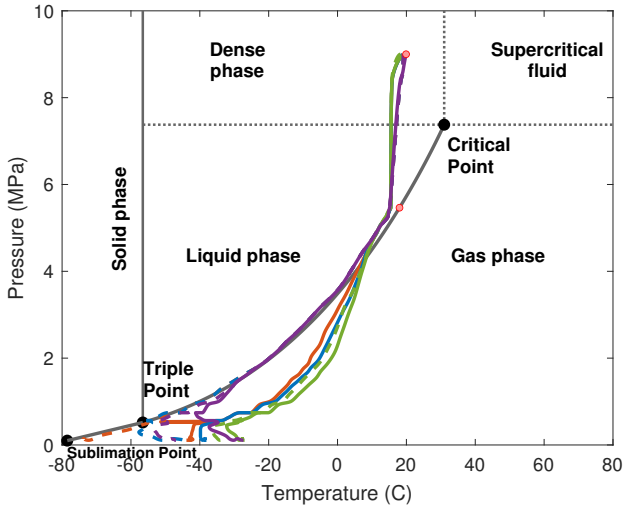

Figure 12 CO_2 **phase diagram showing pressure and temperature during dense phase experiment.**

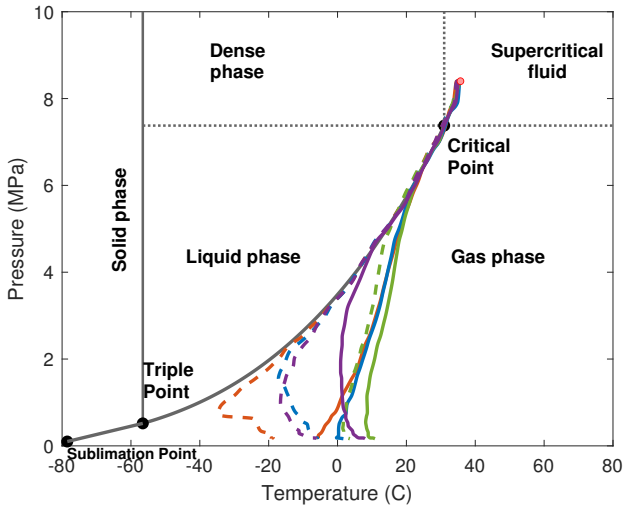

Figure 13 CO_2 **phase diagram showing pressure and temperature during supercritical fluid experiment.**

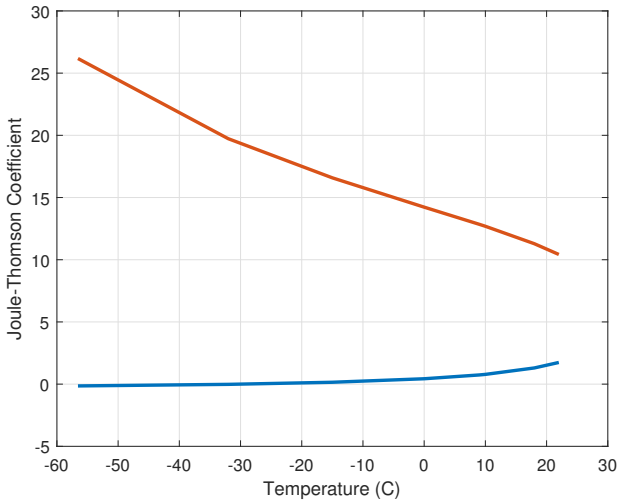

Figure 14 Joule-Thomson coefficient for liquid (blue line) and gas (red line).

the sublimation from gaseous phase to solid phase causes the formation of dry ice.

During the last test with the initial phase of supercritical fluid, first the pressure and temperature drop to the critical point and follow the saturation curve. Subsequently the supercritical fluid changes phase into liquid-vapor before the deviation from the saturation curve to the gas phase.

Figures 15 and 16 show CO_2 T-S diagram. The reference states are 200 KJ/Kg for enthalpy, and 1 $KJ/Kg.K$ for entropy at 0 ºC for saturated liquid.

The phase transitions can be understood better through following the path that the fluid goes through during the experiments. For the test with the initial state of dense phase (A) as shown in figure 15, the fluid rapidly reaches the saturation state (B) and its phase changes from liquid to gas-liquid mixture. As the pressure and temperature drop, the fluid sustains the saturation state along the pipe. Once the fluid reaches state (C), the top section of the pipe deviates from the saturation curve to the fully gaseous phase, initially at 237.4 m from the orifice, then spread to the orifice and finally the whole pipe cross section at 237.4 m. The fluid at the close end of the pipe follows the saturation curve to the state (D) where the deviation from the saturation occurs. At last the fluid at the bottom of the pipe reaches state (E), the triple point, and changes the phase from gas-liquid mixture to solid resulting in the formation of the dry ice at the bottom of the pipe. The measured temperature and pressure at 7.4 m from the orifice shows that the fluid closer to the orifice does not deviate from the saturation curve and reaches the triple point at which gas-liquid-solid are present and after that follows the sublimation curve.

The corresponding temperatures and pressures for the states A to E are presented in table 5 for both dense and supercritical experiments.

The T-S diagram for the test with the supercritical fluid is presented in figure 16. After the inception of the leak

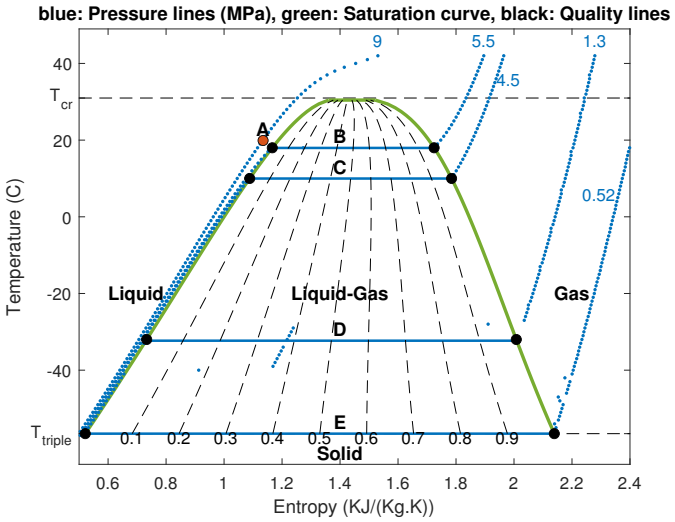

Figure 15 CO_2 **T-S diagram during dense phase experiment.**

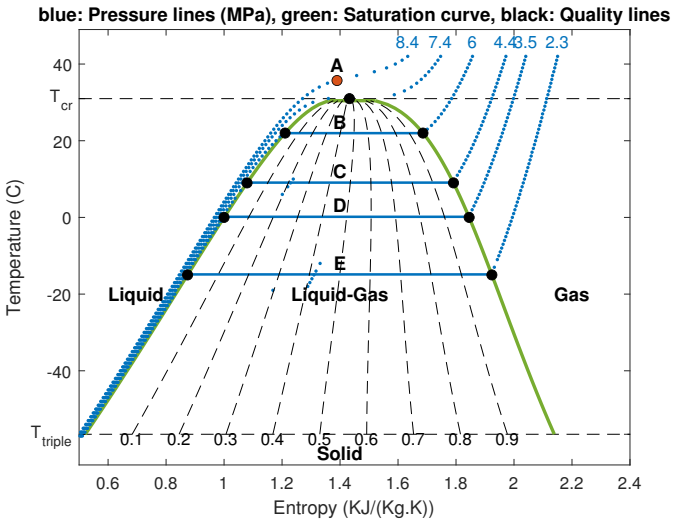

Figure 16 CO_2 **T-S diagram during supercritical phase experiment.**

the fluid reaches the critical point from its initial state and subsequently follows the saturation curve up until state (B). Similar to the dense phase experiment at this point the fluid at the top starting from 237.4 m toward the orifice changes the phase to the gas as well as the bottom section at 237.4 m. Next, the top section of the closed end of the pipe deviates from the saturation curve at state (C). The fluid at bottom section of the pipe remains as liquid-gas mixture before reaching state (D) where the phase transition to gas occurs. Finally the phase change to gas happens for the fluid at the bottom section of the pipe closer to the orifice when it reaches state (E).

Similar to Temperature-Entropy (T-S) diagram, Pressure-Enthalpy (P-h) diagram as demonstrated in figures 17 and 18 can also help understanding the phase transition during the leak.

Table 5 (Temperature, Pressure) values during the experiments

	Dense	Supercritical
A (initial)	$(19.9C, 9MPa)$	$(35.7C, 8.4MPa)$
B (saturation)	$(18C, 5.46MPa)$	$(22C, 6MPa)$
C (saturation)	$(10C, 4.5MPa)$	$(9C, 4.4MPa)$
D (saturation)	$(-32C, 1.33MPa)$	$(0C, 3.5MPa)$
E (saturation)	$(-56.6C, 0.52MPa)$	$(-15C, 2.3MPa)$

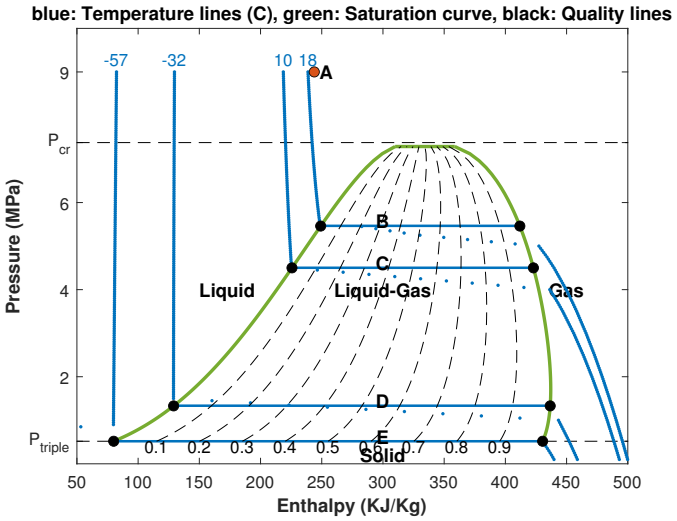

Figure 17 CO_2 **P-h diagram during dense phase experiment.**

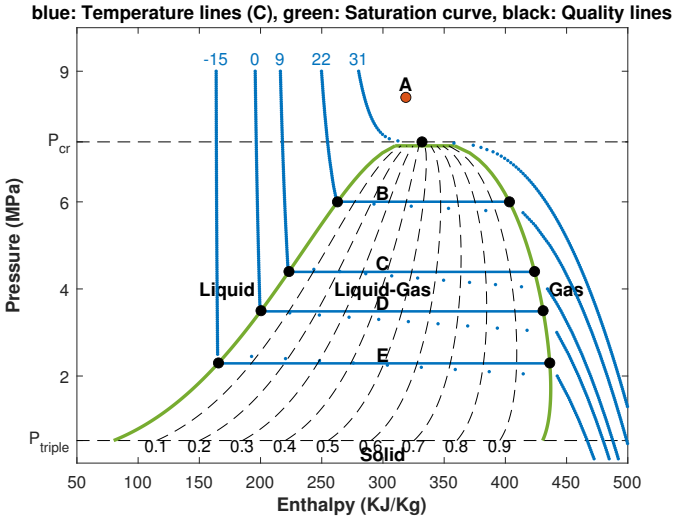

Figure 18 CO_2 **P-h diagram during supercritical phase experiment.**

3.1 Leak Flow Analysis

When CO_2 escapes from a leak hole in a pressurized pipeline, the jet flow structure may exhibit a phenomenon known as a Mach disk, which occurs when the flow reaches sonic conditions at the exit of the leak hole. it means that the flow velocity at the exit of the nozzle reaches the speed of sound

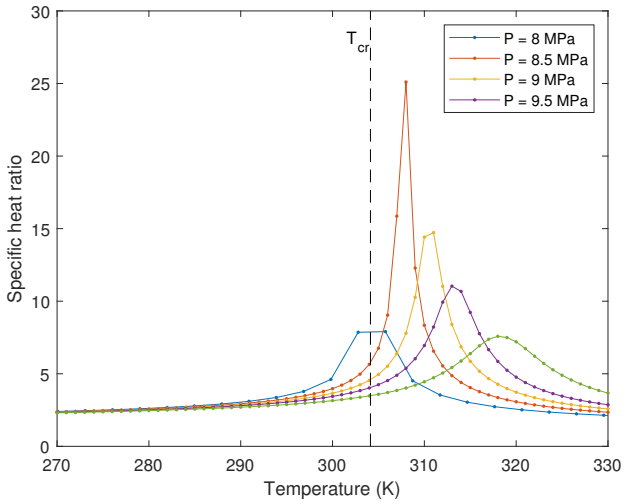

Figure 19 Temperature dependency of specific heat ratio.

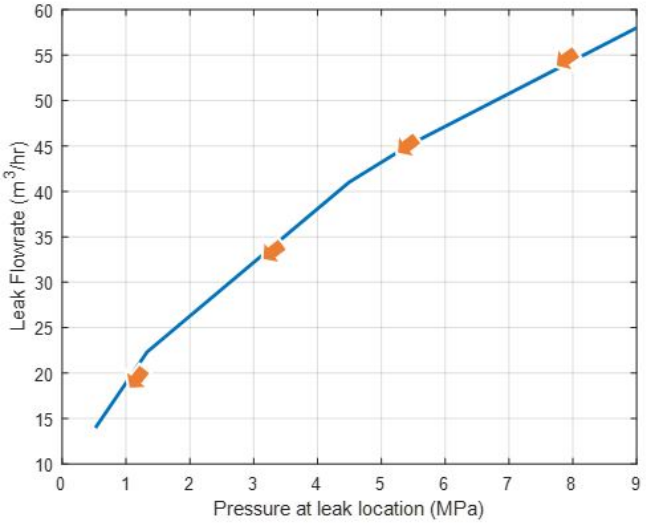

Figure 20 Changes in leak flow rate as the pressure drops.

(c_g), hence the Mach number (M), as defined in equation 3.1, is equal to 1.

$$M = \frac{v}{c_g} \qquad c_g = \sqrt{\gamma RT} \tag{3.1}$$

Equations 3.2, 3.3 and 3.4 describe the relationship between total and static properties of the fluid flow as it passes through a nozzle. These isentropic flow equations can be used assuming the gas is perfect i.e. the specific heat ratio remains constant or only slightly changed across the temperature range. Figure 19 shows the specific heat ratio is almost constant for temperatures below the critical point ($T < 31C$).

Analyzing these equations can capture how changes in pressure, temperature, and density occur as the flow accelerates through the nozzle, ultimately leading to choked flow conditions when the Mach number reaches 1.

$$\frac{P_t}{P} = \left(1 + \frac{\gamma - 1}{2} M^2\right)^{\frac{\gamma}{\gamma - 1}} \tag{3.2}$$

$$\frac{T_t}{T} = \left(1 + \frac{\gamma - 1}{2} M^2\right) \tag{3.3}$$

$$\frac{\rho_t}{\rho} = \left(1 + \frac{\gamma - 1}{2} M^2\right)^{\frac{1}{\gamma - 1}} \tag{3.4}$$

The critical pressure ratio (π_{0b}) can be calculated from equation 3.5 at which the flow through the nozzle becomes choked. It signifies the maximum possible pressure ratio that can be achieved across the nozzle for sonic conditions. When the pressure ratio from equation 3.2 exceeds this critical value, the flow becomes choked.

$$\pi_{0b} = \left(\frac{\gamma + 1}{2}\right)^{\frac{\gamma}{\gamma - 1}} \tag{3.5}$$

The mass flow rate through the leak hole can be calculated using equation 3.6. The mass flow rate through the nozzle reaches its maximum value for a given upstream condition, when the flow is choked ($M = 1$). At this point, further increases in upstream pressure will not result in an increase in mass flow rate, as the flow is already choked.

$$\begin{aligned} \dot{m} &= \rho v A = PMA\sqrt{\frac{\gamma}{RT}} \\ &= P_t M A \sqrt{\frac{\gamma}{RT_t}} \left(1 + \frac{\gamma - 1}{2} M^2\right)^{-\frac{\gamma + 1}{2(\gamma - 1)}} \end{aligned} \tag{3.6}$$

Figure 20 shows the decrease in the leak flow rate as the pressure drops in the pipeline for the dense phase experiment.

3.2 Jet Structure

As CO2 accelerates through the leak hole and reaches sonic conditions, a shock wave forms perpendicular to the flow direction at the exit. This shock wave is known as the Mach disk and marks the boundary between supersonic flow inside the jet and subsonic flow outside the jet.

The Mach disk creates a distinctive shock structure within the jet flow. Behind the Mach disk, the flow transitions from supersonic to subsonic, leading to compression and increased pressure. Ahead of the Mach disk, the flow remains supersonic, characterized by rapid expansion and low pressure.

The presence of the Mach disk influences the expansion and entrainment characteristics of the CO2 jet. The rapid expansion of the flow behind the Mach disk leads to increased

jet width and lateral spreading. At the same time, the shock wave enhances the entrainment of surrounding air into the jet, intensifying turbulence and mixing.

The Mach disk shock wave interacts with ambient air, causing compression and disturbance in the surrounding flow field. This interaction contributes to the dispersion and lateral spreading of the CO2 plume as it travels away from the leak hole.

The Mach disk results in an elevated pressure gradient behind the shock wave. This pressure gradient drives the forward motion of the CO2 jet and influences the trajectory and behavior of the plume.

The presence of a Mach disk may be accompanied by a distinctive sound signature, characterized by a sudden change in acoustic properties as the flow transitions from supersonic to subsonic. This sound signature can aid in the detection and localization of the leak.

4 CONCLUSION

In conclusion, this paper addresses the need for real-time transient modeling of CO_2 pipelines, particularly focusing on the challenges posed by leaks. The proposed modeling framework offers valuable insights into the complex phenomenon of CO_2 release, enhancing our understanding of flow characteristics under various operating conditions.

The findings of this study have significant implications for the development and implementation of robust leak detection systems and the optimization of pipeline design for enhanced reliability. By considering CO_2 flow in gas, liquid, and supercritical states, our approach provides a comprehensive analysis of pipeline behavior, crucial for ensuring the safety and efficiency of pipeline operations.

Through mathematical modeling and validation using case studies, we have demonstrated the utility of our approach in accurately predicting CO_2 pipeline behavior, including phase transitions during a leak. Furthermore, our simulations enable the analysis of factors such as choked flow and maximum flow rates, essential for assessing leak severity and informing mitigation strategies.

Overall, the insights presented in this paper contribute not only to the advancement of CO_2 pipeline management but also to the broader field of fluid transportation, with implications for mitigating emissions of greenhouse gases and enhancing the safety and sustainability of industrial processes.

REFERENCES

[1] M. J. Zucrow and J. D. Hoffman, *Gas dynamics, Vol. I*. John Wiley & Sons, 1977.

[2] H. Ghasvari-Jahromi, M. Roxas, and S. Mokamati, "Column Separation in a Shut-In Liquid Hydrocarbon Transmission Pipeline," vol. Volume 3: Operations, Monitoring, and Maintenance; Materials and Joining of *International Pipeline Conference*, 09 2018.

[3] H. Ghasvari-Jahromi, F. Ekram, M. Roxas, and S. Mokamati, "A Mathematical Model for the Spatial Prediction and Temporal Evolution of the Column Separation in a Flowing Hydrocarbon Transmission Pipeline," PSIG Annual Meeting, pp. PSIG–1910, 05 2019.

[4] M. Chaczykowski and A. J. Osiadacz, "Dynamic simulation of pipelines containing dense phase/supercritical co2-rich mixtures for carbon capture and storage," *International Journal of Greenhouse Gas Control*, vol. 9, pp. 446–456, 2012.

[5] H. Ghasvari-Jahromi, F. Ekram, C. Deng, J. Knudson, and S. Mokamati, "Supercritical Fluid Flow in Pipelines - A Dense Phase Case Study," PSIG Annual Meeting, pp. PSIG–2324, 05 2023.

[6] R. Span and W. Wagner, "A New Equation of State for Carbon Dioxide Covering the Fluid Region from the Triple-Point Temperature to 1100 K at Pressures up to 800 MPa," *Journal of Physical and Chemical Reference Data*, vol. 25, pp. 1509–1596, 11 1996.

[7] J. J. Barley, "Simulation of Anthropogenic Carbon Dioxide Transportation in Pipelines," pp. PSIG–2311, 05 2023.

[8] H. Ghasvari-Jahromi, F. Ekram, W. Ali, M. Roxas, and S. Mokamati, "Performance of CPM Based Leak-Detection Algorithms in the Presence of Slack," PSIG Annual Meeting, pp. PSIG–2103, 05 2021.

[9] X. Guo, S. Chen, X. Yan, X. Zhang, J. Yu, Y. Zhang, H. Mahgerefteh, S. Martynov, A. Collard, and S. Brown, "Flow characteristics and dispersion during the leakage of high pressure co2 from an industrial scale pipeline," *International Journal of Greenhouse Gas Control*, vol. 73, pp. 70–78, 2018.

NOMENCLATURE

ρ	Density [Kg m^{-3}]
v	Velocity [m s^{-1}]
D	Pipe diameter [m]
A	Pipe cross-section area [m^2]
m	mass [Kg]
$\dot{m}$	mass flow rate [Kg s^{-1}]
P	Pressure [Pa]
f	friction factor
g	Gravitational acceleration [m s^{-2}]
u	Specific internal energy[J kg^{-1}]

h	Specific enthalpy[J kg^{-1}]
s	Specific entropy[J kg^{-1}K^{-1}]
T	Temperature [K]
q	Specific heat flow rate [J kg^{-1} s^{-1}]
k	thermal conductivity [Wm^{-1}K^{-1}]
$\overline{h}$	convection heat transfer coefficient [Wm^{-2}K^{-1}]
U	Overall heat transfer coefficient [Wm^{-2}K^{-1}]
R_t	Thermal resistance [W^{-1}K]
x	Distance along the pipe [m]
t	Time [s]
α	Pipe inclination angle
R	Universal gas constant [J mol^{-1} K^{-1}]
γ	Heat capacity ratio c_P/c_V
c_P	Specific heat at constant pressure [[J kg^{-1} K^{-1}]
c_V	Specific heat at constant volume [[J kg^{-1} K^{-1}]
M	Mach number v/c_g
c_g	Sonic velocity [m s^{-1}]

AUTHOR BIOGRAPHIES

Hamed Ghasvari-Jahromi is a leading Chief R&D Scientist at Vanmok Leak Detection Technologies Inc., with over 12 years of experience in computational fluid dynamics and mathematical modeling. His Ph.D. research at the University of British Columbia focused on the mathematical modeling of multiphase flows. Hamed has worked across various industries, including oil and gas, chemical, and petrochemical. He holds a patent for predicting pipeline column separations and has published numerous research articles. Hamed's expertise lies in leak detection technologies, column separation prediction models, Real-Time Transient Model (RTTM), and pattern recognition approaches.

Fatemeh Ekram is an R&D scientist at Vanmok Leak Detection Technologies Inc. She has extensive expertise in process simulation, optimization, and control. Over the past 5 years, her focus was on developing leak detection algorithms using a combination of model-based and data-driven techniques. Fatemeh got her B.Sc. and M.Sc. degrees from the Sharif University of Technology and her Ph.D. in Chemical & Biological Engineering from the University of British Columbia in 2016.

Satya Mokamati is the President & CEO of Vanmok Leak Detection Technologies Inc. He is a professional engineer with over 15 years of experience in the oil and gas sector, with in-depth industry knowledge. Prior to founding Vanmok, Satya worked as a subject matter expert in pipeline leak detection at a major midstream pipeline company. Satya holds a Ph.D. in Mechanical Engineering from UBC, Vancouver, and an MS in Mechanical Engineering from UNB, Fredericton. He is a member of APEGA and is dedicated to advancing leak detection technology in the pipeline industry.